International Journal of Heat and Fluid Flow 30 (2009) 877–885

Contents lists available at ScienceDirect

International Journal of Heat and Fluid Flow

journal homepage: www.elsevier.com/locate/ijhff

Time resolved investigations on flow field and quasi wall shear stress of an impingement configuration with pulsating jets by means of high speed PIV and a surface hot wire array

Timm Janetzke *, Wolfgang Nitsche

Berlin Institute of Technology, Department of Aeronautics and Astronautics, Chair of Aerodynamics, Marchstr. 12, 10587 Berlin, Germany

ARTICLE INFO

Article history:
Received 25 November 2008
Received in revised form 12 March 2009
Accepted 17 March 2009
Available online 23 April 2009

Keywords:
Impinging jets
Pulsating jets
Time resolved PIV
Surface hot wires
Heat transfer enhancement

ABSTRACT

The effects of jet pulsation on flow field and quasi wall shear stress of an impingement configuration were investigated experimentally. The excitation Strouhal number and amplitude were varied as the most influential parameters. A line-array with three submerged air jets, and a confining plate were used. The flow field analysis by means of time resolved particle image velocimetry shows that the controlled excitation can considerably affect the near-field flow of an impinging jet array. These effects are visualized as organization of the coherent flow structures. Augmentation of the Kelvin–Helmholtz vortices in the jet shear layer depends on the Strouhal number and pulsation magnitude and can be associated with pairing of small scale vortices in the jet. A total maximum of vortex strength was observed when exciting with $Sr = 0.82$ and coincident high amplitudes.

Time resolved interaction between impinging vortices and impingement plate boundary layer due to jet excitation was verified by using an array of 5 μm surface hot wires. Corresponding to the global flow field modification due to periodic jet pulsation, the impact of the vortex rings on the wall boundary layer is highly influenced by the above mentioned excitation parameters and reaches a maximum at $Sr = 0.82$.

1. Introduction

Impinging jets are used in a variety of aviation applications where high local heat transfer coefficients are needed, e.g. engine turbine blades or combustion chamber liners. As compressor bleeding air is used to cool the mentioned components, overall engine efficiency is reduced. Consequently, a major goal of engine designers is the minimization of the needed coolant mass flow. The actual standard type impingement cooling system uses a steady coolant supply. A large number of studies has shown numerous parameters which affect the convective flow field and wall heat flux, respectively. A useful survey can be found in Pagenkopf (1996). One of the most important phenomena was documented by Kataoka et al. (1987) who showed the potential influence of the circular vortices that generally surround submerged circular jets on heat transfer characteristics of impinging jets. Vortex merging leads to large-scale annular vortices scaling with the nozzle diameter. The impingement of these vortex systems has a strong effect on resulting heat transfer.

A recent approach to enhance the cooling effectiveness of impingement cooling systems is the usage of periodically pulsating jets. Far fewer studies concerning unsteady jets exist and results are quite non-uniform, as enhancement of heat transfer is observed or not (e.g. Camci and Herr, 2002; Herwig et al., 2004; Zumbrunnen and Aziz, 1993). A fundamental study concerning perturbation growth in round free jets was done by Zaman and Hussain (1980). It was shown, that maximum augmentation rates exist at an excitation Strouhal number of $Sr = 0.3$, whereas absolute maximum velocity fluctuations are generated when exciting with $Sr = 0.8$. This was explained with an enhanced vortex roll-up due to effective jet excitation. An analytic estimation of a useful boundary layer renewal frequency at the impingement plate surface that leads to enhanced heat transfer rates was introduced by Zumbrunnen and Aziz (1993). The derived minimum renewal Strouhal number of $Sr = 0.26$ was confirmed for a non-submerged water jet and later on for a submerged air jet by Hofmann (2005). The former of these two studies excluded any shear layer effects, whereas in the latter study shear layer effects occured, but no sufficient fluid dynamical explanation of the detected heat transfer enhancement was given. In Janetzke et al. (2008) the potential of enhancing cooling effectiveness due to an effective augmentation of the above mentioned vortex systems was verified by the combined usage of time-mean selective temperature measurements, phase-triggered particle image velocimetry and qualitative time-mean surface visualizations. Geometric factors of real application configurations were taken into account by using a metallic impingement plate, a nozzle array and a flow confinement. The actual study extends our

* Corresponding author. Tel.: +49 30 314 21321.
E-mail address: Timm.Janetzke@ILR.TU-Berlin.de (T. Janetzke).

0142-727X/$ - see front matter © 2009 Elsevier Inc. All rights reserved.
doi:10.1016/j.ijheatfluidflow.2009.03.006

Nomenclature

d	nozzle diameter (m)
e	AC voltage (V), "quasi" wall shear stress
f	frequency (Hz)
j	index (−)
l	nozzle length (m)
N	number of time traces (−)
Re	Reynolds number (−), $Re = \frac{v_{DIA} \cdot d}{\nu}$
Sr	Strouhal number of excitation (−), $Sr = \frac{f \cdot d}{v_{DIA}}$
t	time (s)
u	velocity (m/s)
v	instantaneous jet exit velocity (m/s)
$\|v\|$	absolute velocity (m/s)
v^*	dimensionless velocity (−), $v^* = \frac{\|v\|}{\|v\|_{mean,0Hz}}$
x	radial distance perpendicular to the nozzle axis (m)
y	nozzle-to-plate distance (m)
ε	cooling effectiveness (−), $\varepsilon = \frac{T_{Wall} - T_{Hot}}{T_{Hot} - T_{Cold}}$
ϵ_{bias}	PIV bias error (m/s)
γ_2	excess kurtosis of the AC signal (−)
σ	standard deviation of the AC signal (V)
μ_4	4^{th} moment about the mean of the AC signal $[V^4]$
ω_z	vorticity (1/s)
ω_z^*	dimensionless vorticity (−), $\omega_z^* = \frac{\omega_z \cdot d}{\|v\|_{mean,0Hz}}$

Subscripts/superscripts

0 Hz	without excitation
DIA	average over nozzle diameter
EX	with excitation
mean	time-mean
P	periodic
SP	stagnation point
$'$	fluctuation
$\hat{}$	ensemble averaged
$*$	dimensionless

former results such that high speed PIV measurements in combination with time resolved quasi wall shear stress measurements document the periodic disruption and renewal of the impingement plate boundary layer.

2. Experimental study

Fig. 1 shows the experimental setup used for the PIV measurements. To avoid gravity influences, a layout with vertically impinging jets was chosen. Opposite the impingement plate the confining wall holds the 3-nozzle-line-array. The nozzles themselves have an aperture diameter of $d = 12$ mm and a ratio of length/diameter $l/d = 2.5$. The nozzle design is oriented toward reality by using simple drill holes. A constant dimensionless nozzle-to-plate spacing of $y/d = 2$ is used and the spacing between two adjacent nozzles is kept constant at $spacing/diameter = 5$ too. The coolant mass flow is taken from a compressed air reservoir and adjusted automatically with a calibrated thermical flow meter in combination with a computer controlled valve. Steady-state flow conditions at the flow meter are ensured with the integration of a damping chamber between flow meter and pulsation generator. The computer controlled actuator allows an excitation with frequencies up to $f_{EX} = 700$ Hz. Further details of the actuator mechanism can be found in Janetzke et al. (2008).

The TR-PIV system consists of a second harmonic Nd:YLF high speed laser, a CMOS high speed camera, a synchronizer unit, a variable light arm and the lightsheet optics, providing a minimum lightsheet thickness of 0.5 mm. The laser system allows repetition frequencies up to 10 kHz per cavity. The available frame rate of the camera system depends on the size of the desired investigation window which is shown in Fig. 1. The window dimensions were chosen to allow the simultaneous observation of the dynamic jet shear layer phenomena as well as the forced vortex-surface interaction at the wall. The used camera resolution of 475×288 pixels yields a pixel size of 0.083 mm as the calibration was done for a 39.6×24 mm image section. Pulse repetition frequency was set to 6500 Hz which is 10 times the maximum excitation frequency resulting in a corresponding camera frame rate of 13,000 fps. The flow was seeded with DEHS particles and images were recorded for further evaluation. Related frames were cross-correlated using the commercial ILA VidPIV code which offers advanced interrogation window shifting and window deformation techniques (Adrian, 1986; Huang et al., 1993). The use of subpixel analysis methods reduces the mean bias error to 1/10th–1/20th of the pixel size (Raffel et al., 2007). In the present case the time difference between two successive frames is $\Delta t = 25$ μs, which yields a theoretical error of 0.16 m/s < ϵ_{bias} < 0.332 m/s. Spurious velocity vectors were typically 5% of the total vector count. An uncertainty analysis based on Raffel et al. (2007) estimates a typical velocity uncertainty of 5% and a vorticity uncertainty of 7–8%.

The TR-PIV measurements were supplemented with transient data of the boundary layer footprint at the impingement plate by using an array of 5 μm surface hot wires (SHW). Fig. 2 shows the design and dimensions of a single sensor. The platinum SHW with a diameter of 5 μm is stretched over a cavity which is 2.5 mm long, 100 μm wide and 35 μm deep. Both ends of the SHW are welded onto the 35 μm thick copper layer that is located upside an epoxy substructure. Due to the considerably reduced heat losses into the wall compared to conventional surface hot films, SHW show an improved signal to noise ratio combined with higher critical frequencies (Sturzebecher et al., 2001; Burkhardt et al., 2001). The setup for the transient wall shear stress measurements including the used sensor array layout and sensor positioning below the nozzle array can be seen in Fig. 3. The hot wires were operated in CTA mode using a multi channel hot wire anemometer and a 16 bit A/D-converter card. The CTA voltage signal was split into AC and DC parts to isolate the actively generated oscillation from the mean component. Sampling rate was set to 20 kHz and the number of samples was adapted to the excitation frequency to include five periods of the excitation signal. The instantaneous AC velocity signal consists of the periodic oscillation v_P and the stochastic fluctuation v'.

$$v(t) = v_P + v' \tag{1}$$

The usage of a phase-locked ensemble averaging technique according to Evans (1975) with $N = 500$ single measurements minimizes the stochastical component and results in a low noise ensemble averaged time trace $\hat{v}(t)$ which represents the oscillating signal component.

$$\hat{v}(t) = \frac{1}{N} \sum_{j=1}^{N} v_j(t) \tag{2}$$

As manually produced surface hot wires show individual reactions to occurring flow fluctuations, a reference RMS vector was acquired using an artificially generated disturbance of known amplitude. The corresponding maximum RMS value was acquired for each SHW sensor and all sensors were scaled with the RMS value of the stagnation point hot wire. Thus, the signal response of

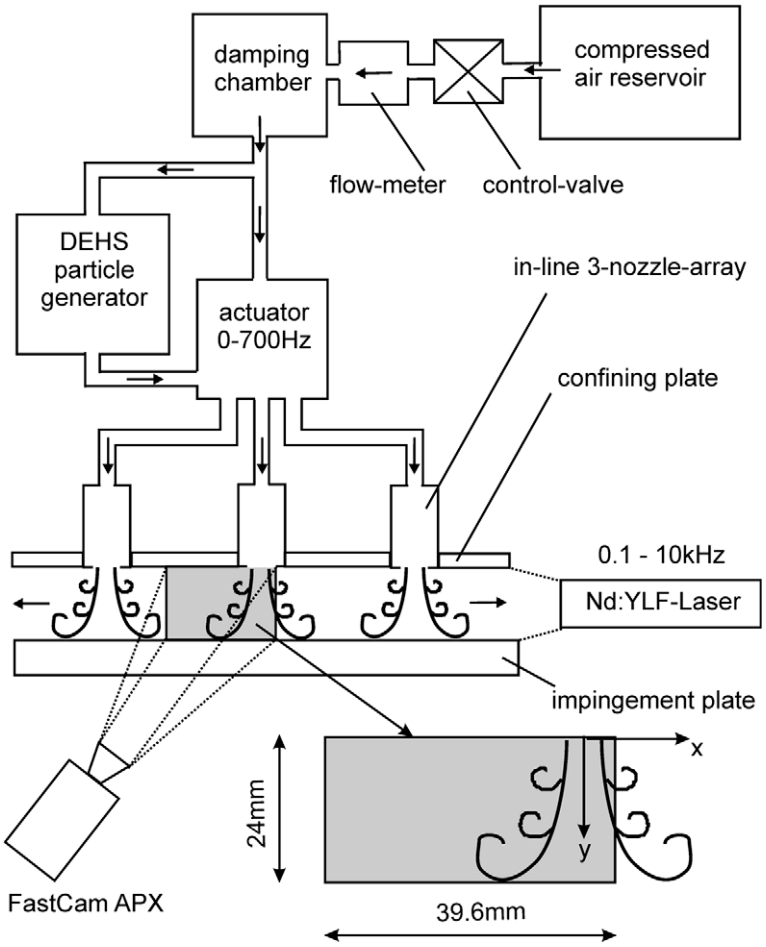

Fig. 1. Experimental setup and investigation window of the TR-PIV measurements.

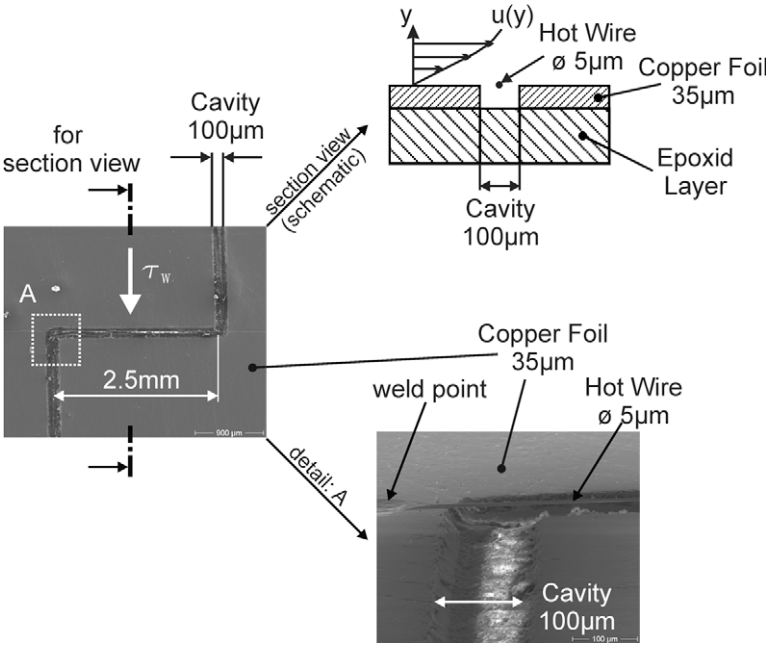

Fig. 2. Surface Hot Wire. top: schematic view of the general layout. Center: magnified topview of a single SHW stretched over the cavity. Bottom: detail view of the SHW with appropriate weld point.

the whole sensor array could be adequately equalized. Calibrating SHW arrays is very time-consuming, as the calibration reference must provide a sufficiently high spatial resolution and different calibrations for laminar and turbulent boundary layers must be

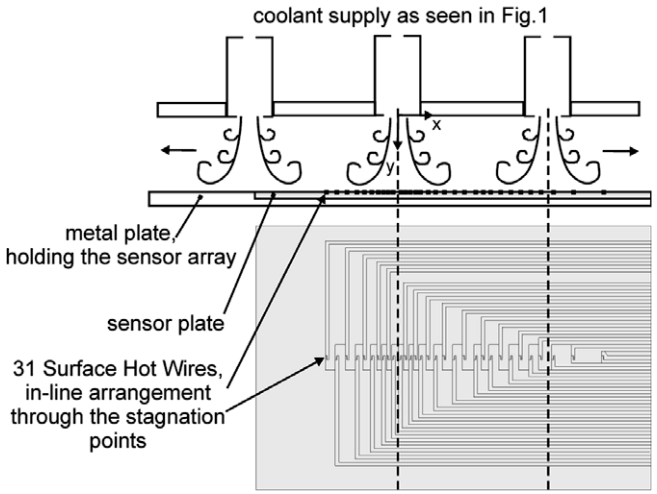

Fig. 3. Layout of the used SHW array and sensor positioning at the impingement plate below the nozzles.

made. However, the detection and comparison of actively generated oscillations can be done without the necessity to calibrate the sensors. For that reason, the raw ensemble averaged AC voltage signals $e[V]$ were used. Due to the measurement principle which directly correlates the sensor voltage and wall shear stress, the sensor signals can be termed as "quasi" wall shear stress. The identification of characteristic phenomena like boundary layer separation or propagating coherent structures can be made by using the excess kurtosis γ_2,

$$\gamma_2 = \frac{\mu_4}{\sigma^4} - 3 \tag{3}$$

where μ_4 is the fourth moment about the mean and σ is the standard deviation (Joanes and Gill, 1998). γ_2 describes the shape of the distribution of measured data compared to the standard Gaussian distribution. $\gamma_2 > 0$ indicates a sharper and higher peak with fatter tails whereas $\gamma_2 < 0$ identifies a rounded peak with wider shoulders. Thus, in the case of recorded AC signals, $\gamma_2 > 0$ is an indicator for extreme values that occur more frequently than "normal". As large coherent flow structures induce a sharper and higher SHW signal response than for example broadband turbulence phenomena, they can be identified by values of $\gamma_2 > 0$.

The investigated operation points were selected upon the results of the thermal measurements in Janetzke et al. (2008) which

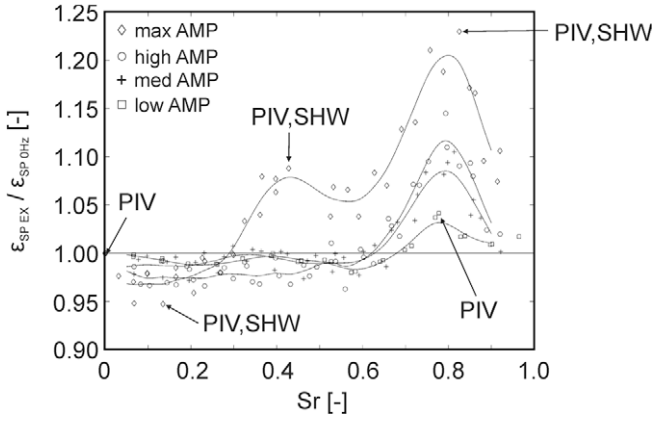

Fig. 4. Enhancement rates of stagnation point cooling effectiveness due to jet pulsation as a function of Strouhal number and pulsation magnitude, $Re = 7280, y/d = 2$, see (Janetzke et al., 2008).

are summarized in Fig. 4. As illustrated, a maximum enhancement rate of stagnation point cooling effectiveness up to 20% could be achieved when exciting with $Sr = 0.82$, whereas reductions up to 5% occured at low Strouhal numbers. Enhancement as well as reduction was maximum at the highest excitation level. Furthermore, a local maximum of cooling effectiveness was observed at $Sr = 0.41$ which is the subharmonic of the optimum excitation frequency. During the experiments the Reynolds number was kept constant at $Re = 7280$. The TR-PIV measurements were made at four significant Strouhal numbers $Sr = 0, Sr = 0.136, Sr = 0.41$ and $Sr = 0.82$ with maximum pulsation level. Additionally, excitation level was reduced at $Sr = 0.82$. The SHW measurements were made at the operation points $Sr = 0.136, Sr = 0.41$ and $Sr = 0.82$ with maximum excitation amplitude exclusively.

3. Results and discussion

As a reference for the following TR-PIV measurements with pulsating jet flows Fig. 5a shows the instantaneous dimensionless velocity field in the vicinity of the center nozzle with steady coolant feed. Jet phenomenology corresponds with literature (Viskanta, 1993) with a dimensionless jet core velocity of $v^* = 1$ at the nozzle exit. Along the centerline the jet is deaccelerated to $v^* = 0$ at the stagnation point whereas the outer jet zones are deflected parallel to the wall. At $x/d = 2.5$ the wall jets of the two adjacent nozzles collide and force the flow into a large circular motion.

Due to the high velocity gradients in the jet shear layer, Kelvin–Helmholtz vortices are formed behind the nozzle aperture, which can clearly be seen in the plot of dimensionless vorticity ω_z^* in Fig. 5b. Initially, the vortices scale with the momentum thickness of the boundary layer at the nozzle lip. Subsequently, the small scale structures roll-up to large vortex systems scaling with the nozzle diameter and propagate with a natural Strouhal number of $Sr = 0.3$–0.5 (Crow and Champagne, 1971). The impact of these structures at the wall has large influence on resulting heat transfer characteristics due to boundary layer renewal effects (Kataoka et al., 1987), although the instantaneous time traces at the points P_1 and P_2 in Fig. 5c and d show, that the induced natural velocity fluctuations are rather limited.

Fig. 6a–e shows the modified instantaneous flow field at fixed time increments when the jets pulsate with $Sr = 0.136$ and highest excitation level which is the most ineffective operation point as cooling effectiveness is reduced by 5% compared to steady coolant supply (see Fig. 4). The time resolved images allow the direct tracking of the actively generated vortices. Vortex size has considerably increased but the roll-up process is quite ineffective as vortex pairing has not completed until the vortex systems impinge at the wall. A comparison of the time traces in Figs. 10 and 5c), Fig. 12 illustrates the increased fluctuation level due to the actively generated vortex rings. In general, the impingement of a sufficiently strong vortex ring at the wall induces a counter rotating secondary vortex which is considerably smaller than the impinging vortex (Walker et al., 1987). Vorticity is distinctly higher with inverse sign. The secondary vortex is directly adjacent to the large primary vortex which forces the secondary vortex into a further rotational motion off the wall followed by the merging of the two vortices. This dynamic interaction is marked in Fig. 6c–e. The Campbel plot of the transient SHW fluctuation signal in Fig. 14a identifies the existence of several unpaired vortices directly at the wall too, showing four shear stress maxima per excitation period. In contrast to the PIV plots which allow the direct identification of the primary and corresponding secondary vortices in terms of positive and negative vorticity, the boundary layer footprint shows the transient wall shear stress as a result of both the primary and the secondary vortices as positive values. However, the Campbel plot of the excess

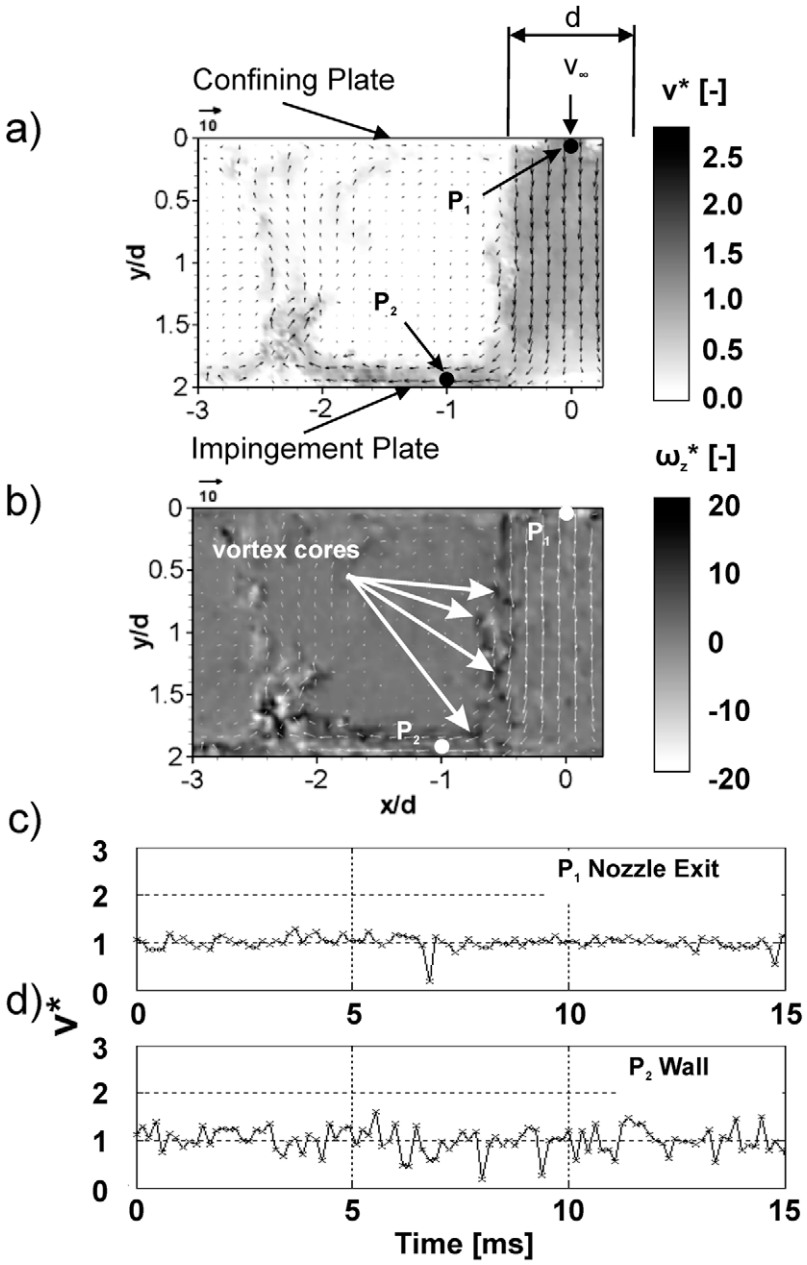

Fig. 5. Steady reference $Sr = 0$. Dimensionless velocity (a). Dimensionless vorticity (b). Time traces of dimensionless velocity at the nozzle exit (c) and near the wall (d).

kurtosis γ_2 in Fig. 15 makes it possible to identify primary and secondary vortices. The large primary vortices as well as the smaller secondary vortices cause a $\gamma_2 > 0$ which results in twice the number of maxima occurring in the excess kurtosis plot compared to the shear stress plot. Note that in the region where the wall jets collide and a second stagnation region with boundary layer separation is formed $(x/d \approx 2.5)$, the excess kurtosis γ_2 shows positive values, too. This is due to the periodic pulsation of this region in size, which is governed by the oscillatorically appearing vortex structures. As the mean value in this region is close to zero, even a moderate pulsation leads to high values that occur more frequently than normal.

An excitation with $Sr = 0.41$ leads to an increase in vortex strength and size (Fig. 7a–e), whereas vortex merging still remains incomplete. The oscillating velocity signal at the nozzle exit (P_1) reaches values of twice the mean core velocity of the steady jet. One millimeter off the wall (P_2), the peak velocity exceeds the naturally generated fluctuation by 50% (Fig. 11). This seems to be of similar level compared to the excitation with $Sr = 0.136$. But, when looking at the Campbel plot in Fig. 14b the wall shear stress fluctuation is clearly higher. This illustrates the necessity of the additional SHW measurements which yield results directly at the wall. As a conclusion, the strengthened vortex rings get closer to the wall which intensifies the boundary layer renewal process, resulting in a plus of stagnation point cooling effectiveness of 8%. This is owed to the specific timing of the dynamic vortex interaction at this operation point, which is illustrated in Fig. 7b–d. A first medium-size vortex (A) is generated which propagates downstream. On its way to the impingement plate, the diameter of the vortex grows, respectively. Then, a second larger vortex (B) is formed, travelling behind the first vortex and getting accelerated by the clockwise rotation of vortex (A). Due to the smaller diameter and the local flow orientation, vortex (B) is subsequently hurled through the center of vortex (A). Thus, the directly following

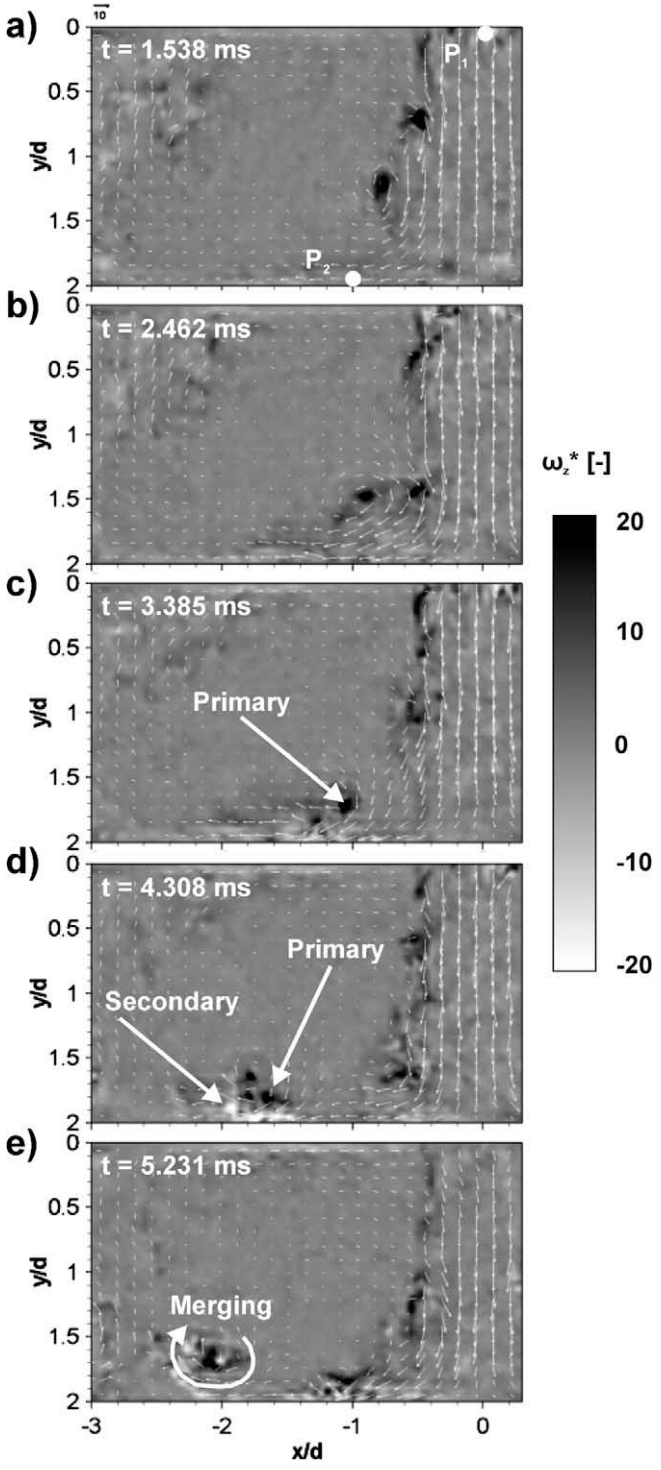

Fig. 6. (a–e) Dimensionless vorticity field, $Sr = 0.136$ Max AMP.

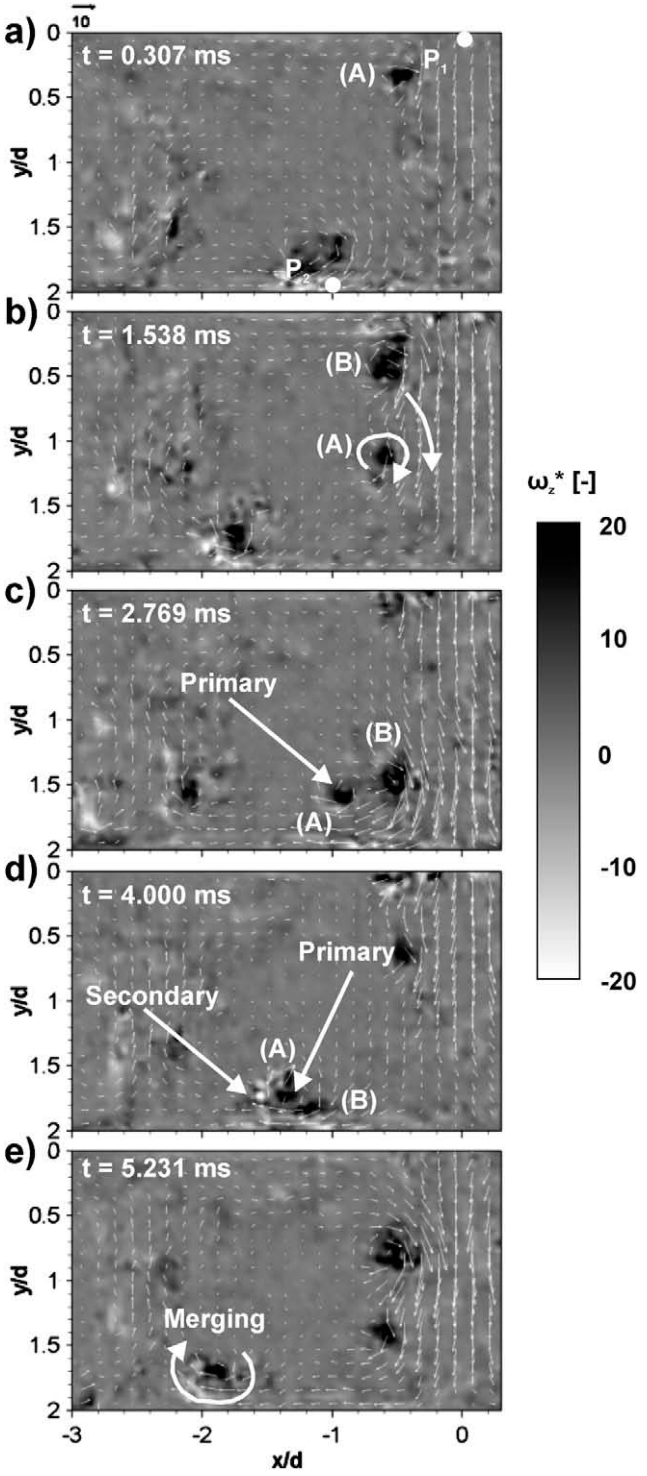

Fig. 7. (a–e) Dimensionless vorticity field, $Sr = 0.41$ Max AMP.

impingement at the wall is of augmented level as can be seen in Fig. 14b which results in the above mentioned heat transfer enhancement rate.

It is worth mentioning that this kind of interaction appeared at several operation points, but with differing timings and distances to the impingement plate, respectively. However, according to Janetzke et al. (2008) heat transfer enhancement could only be observed in those cases, when the hurling of the second vortex through the first one was directly followed by the impingement process. This is evident, as a vortex that is hurled through another one too soon is subsequently forced back into a large circulation off the wall. Thus, the temporal profit in momentum directed to the wall is lost again, whereas a well timed hurling takes full advantage of the additional velocity amount as seen above.

Fig. 8a–e shows the completely different flow field that results when the excitation Strouhal number is raised to $Sr = 0.82$. Vortex pairing is very effective and almost completed directly at the nozzle aperture, resulting in very large annular vortices with very high vorticity levels. This is substantiated with the time trace in Fig. 12 that shows velocity peaks of 2.3 times of the steady case mean

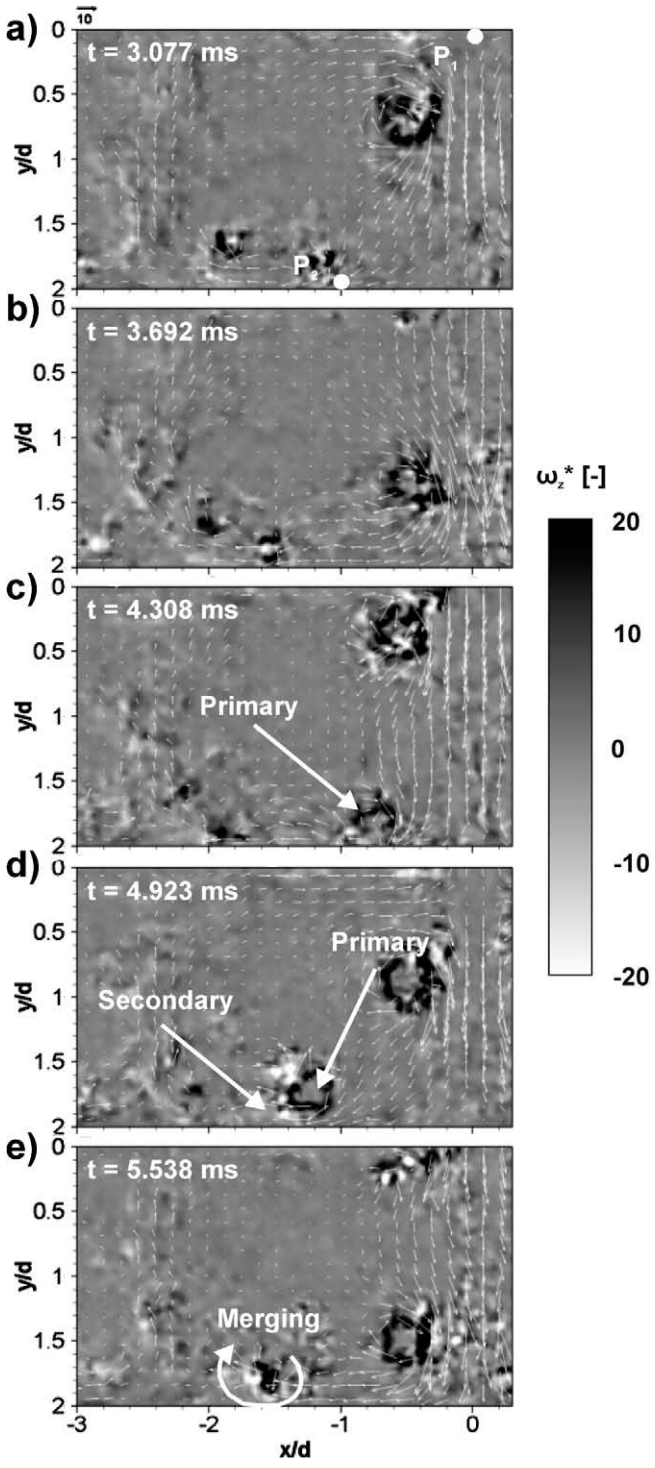

Fig. 8. (a–e) Dimensionless vorticity field, $Sr = 0.82$ Max AMP.

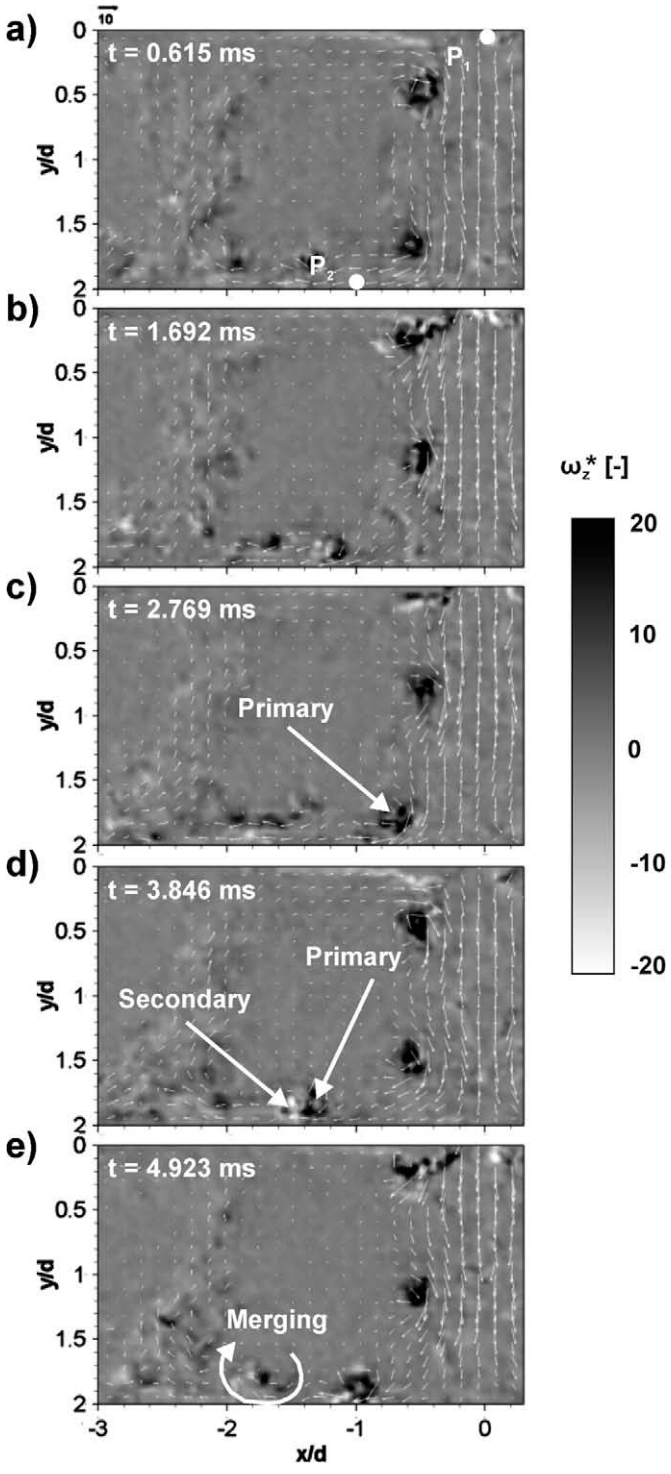

Fig. 9. (a–e) Dimensionless vorticity field, $Sr = 0.82$ Low AMP.

velocity in the jet core at P_1. Due to the high vortex strength, the boundary layer at the wall is periodically disrupted and regenerated which results in very high transient wall shear stress which is confirmed by the Campbel plot in Fig. 14c. At point P_2 in Fig. 12 which is 1 mm off the wall, the velocity periodically drops close to zero, as the strong vortex systems are so close to the wall that the vortex cores are detected when passing this point. Correspondingly, the excess kurtosis γ_2 in Fig. 15c shows strong primary and resulting secondary vortex tracks. Concerning heat transfer, the boundary layer renewal effects clearly dominate the mixing effects which leads to an enhancement of stagnation point cooling effectiveness of 20% compared to the steady reference (Fig. 4).

When reducing pulsation level at the most effective operation point of $Sr = 0.82$, heat transfer enhancement drops from 20% to 4% (Fig. 4). Figs. 9a–e and 13 show that vortex pairing remains very effective. However, the lower pulsation level leads to a weaker interaction between vortices and surface boundary layer which results in lower heat transfer. This makes clear, that both influencing excitation parameters, frequency and pulsation level, must be tuned together to achieve higher heat transfer rates compared to steady jets.

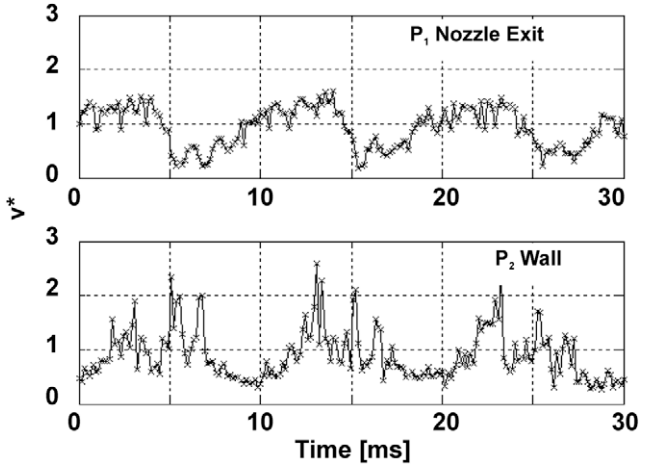

Fig. 10. Dimensionless velocity time traces, $Sr = 0.136$ Max AMP at the nozzle exit (top) and near the wall (bottom).

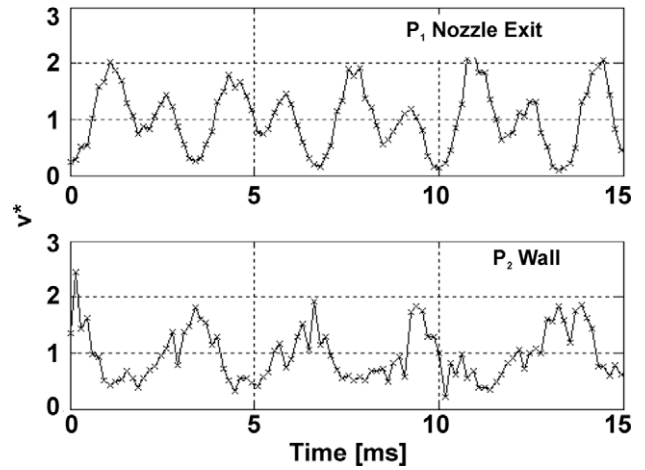

Fig. 11. Dimensionless velocity time traces, $Sr = 0.41$ Max AMP at the nozzle exit (top) and near the wall (bottom).

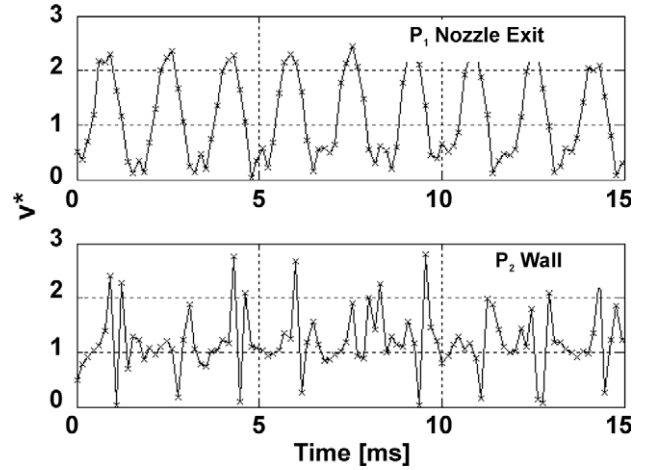

Fig. 12. Dimensionless velocity time traces, $Sr = 0.82$ Max AMP at the nozzle exit (top) and near the wall (bottom).

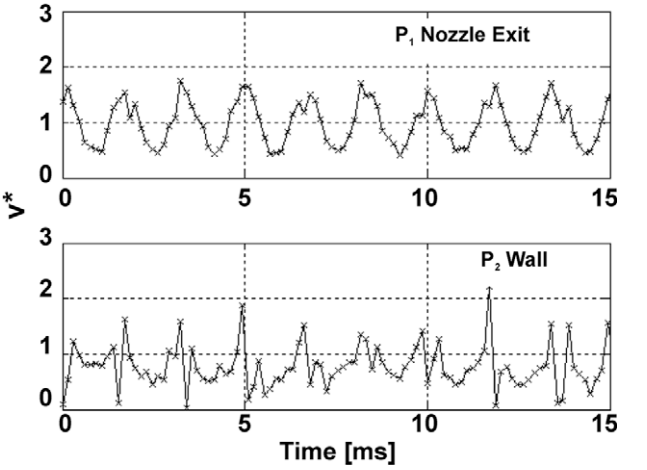

Fig. 13. Dimensionless velocity time traces, $Sr = 0.82$ Low AMP at the nozzle exit (top) and near the wall (bottom).

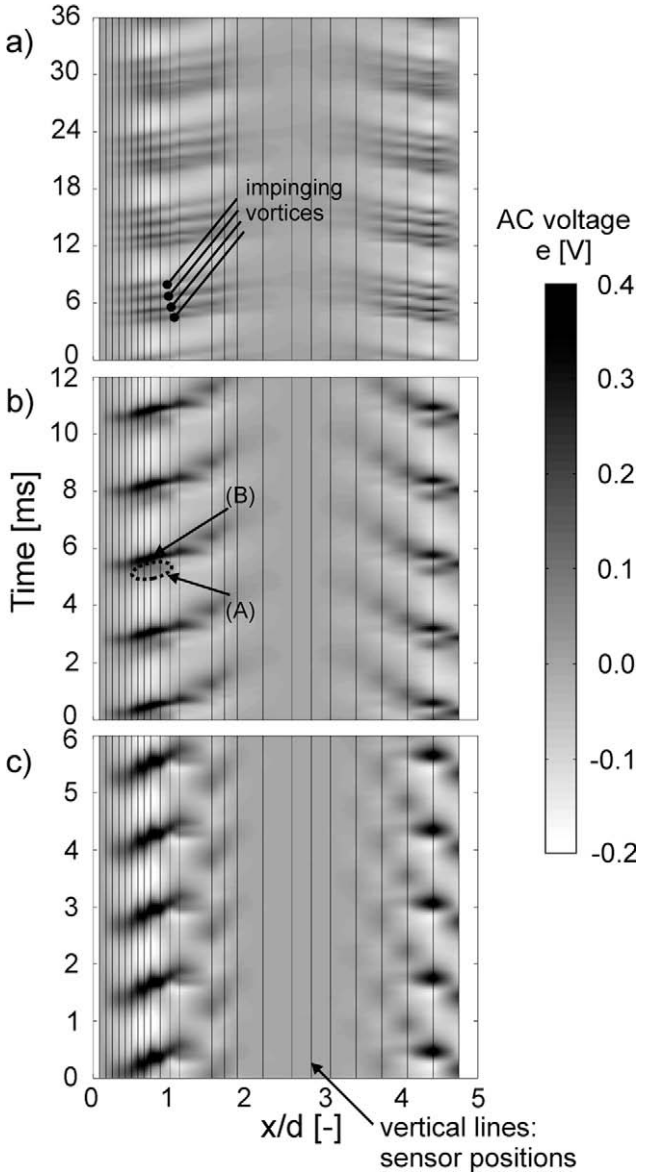

Fig. 14. Campbel plots of quasi wall shear stress. Max AMP. (a) $Sr = 0.136$, (b) $Sr = 0.41$, and (c) $Sr = 0.82$.

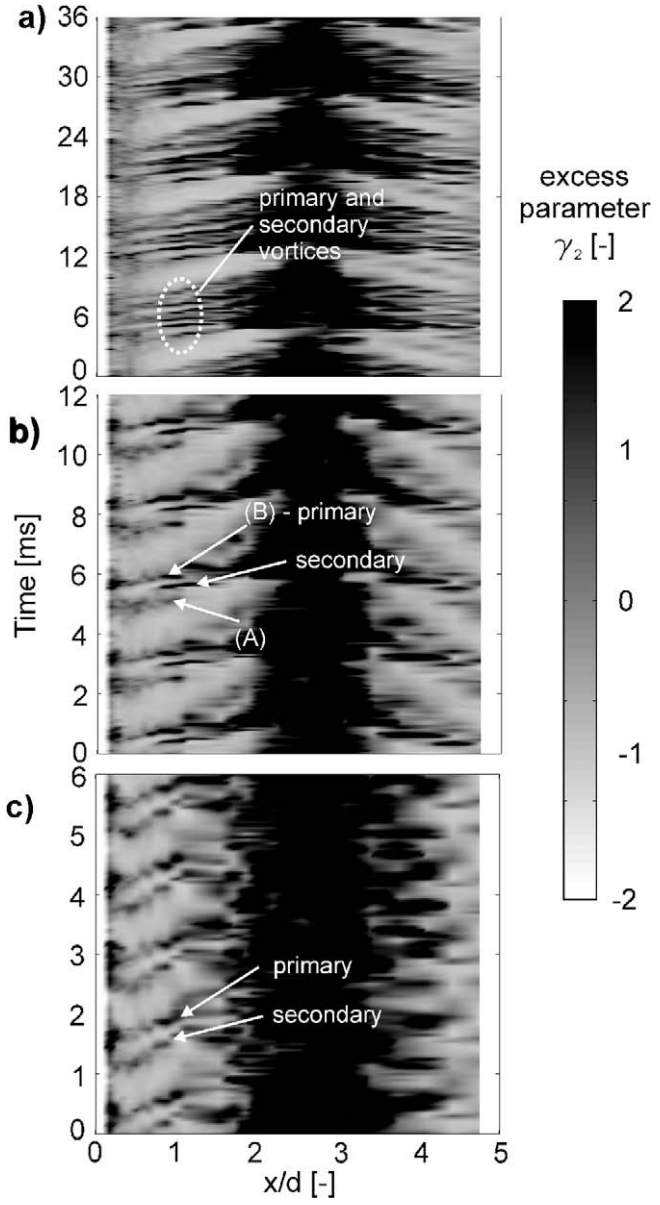

Fig. 15. Campbel plots of excess kurtosis γ_2. Max AMP. (a) $Sr = 0.136$, (b) $Sr = 0.41$, and (c) $Sr = 0.82$.

4. Conclusions

Combined time resolved investigations on flow field and wall shear stress of a jet impingement configuration were done by means of time resolved PIV and surface hot wires. The TR-PIV measurements allowed the direct tracking of several vortex systems which were actively generated in the jet shear layer and subsequently impinging at the wall. Generally, occurence of actively generated vortices in the jet shear layer was observed at all investigated operation points, whereas effectiveness of vortex merging and resulting vortex strength showed a strong dependance of excitation frequency and amplitude.

Vortex pairing was most effective at an excitation Strouhal number of $Sr = 0.82$ and coincident maximum pulsation amplitude which led to strong vortices that were directly triggered with the excitation frequency. When pulsation level at $Sr = 0.82$ was reduced, vortex roll-up remained effective but vortex strength and size dropped. At all other operation points, vortex merging could not be completed before impinging at the wall. A special case could be observed at the excitation Strouhal number of $Sr = 0.41$, where a medium-size vortex that travelled ahead hurled a following larger vortex against the wall with a resulting increase in impingement amplitude.

Heat transfer characteristics are obviously affected by the interaction between impinging vortices and the boundary layer at the wall. The occurence of secondary vortices at the wall that were induced by the impinging primary vortices could be detected at all operation points. The TR-PIV measurements allowed the direct tracking and identification of primary and secondary vortices outside the boundary layer, whereas the SHW measurements substantiated these results with the corresponding transient footprint of the vortex tracks directly at the wall. Thus, an excitation with $Sr = 0.82$ and maximum pulsation level could be verified as the most influencing operation point, inducing maximum wall shear stress fluctuation which corresponds with our earlier investigations on resulting heat transfer in Janetzke et al. (2008).

Acknowledgements

The results of this study were gained in cooperation with Rolls-Royce Germany Ltd & Co KG from the federal research project Luftfahrtforschungsprogramm-III (Project No. 10024592) which was funded by the German Ministry of Economics and Technology.

References

Adrian, R.J., 1986. An image shifting technique to resolve directional ambiguity in double-pulsed laser velocimetry. Applied Optics 23, 3855–3858.
Burkhardt, O., Dinata, U.G.S., Warsop, C., Nitsche, W., 2001. New developments in surface flow sensor technology within the framework of AEROMEMS. Notes on Numerical Fluid Mechanics 76, 207–217.
Camci, C., Herr, F., 2002. Forced convection heat transfer enhancement using a self-oscillating impinging planar jet. Journal of Heat Transfer 124, 770–782.
Crow, S., Champagne, F., 1971. Orderly structure in jet turbulence. Journal of Fluid Mechanics 48, 547–591.
Evans, R.L., 1975. Turbulence and unsteadiness measurements downstream of a moving blade row. ASME Journal of Engineering for Power 122, 131–139.
Herwig, H., Göppert, S., Gürtler, T., Mocikat, H., 2004. Wärmeübergang bei instationären Prallstrahlen. Chemie Ingenieur Technik 76, 84–88.
Hofmann, H., 2005. Wärmeübergang beim pulsierenden Prallstrahl. Ph.D. Thesis, Universität Karlsruhe.
Huang, H.T., Fiedler, H.E., Wang, J.J., 1993. Limitation and improvement of PIV. Part 1: Limitation of conventional techniques due to deformation of particle image patterns. Experiments in Fluids 15, 168–174.
Janetzke, T., Nitsche, W., Täge, J., 2008. Experimental investigations of flow field and heat transfer characteristics due to periodically pulsating impinging air jets. Heat and Mass Transfer 45 (2), 193–206.
Joanes, D.N., Gill, C.A., 1998. Comparing measures of sample skewness and kurtosis. Journal of the Royal Statistical Society: Series D (The Statistician) 47, 183–189.
Kataoka, K., Suguro, M., Degawa, H., Mihata, I., 1987. The effect of surface renewal due to large-scale eddies on jet impingement heat transfer. International Journal of Heat and Mass Transfer 30, 559–567.
Pagenkopf, U. 1996. Untersuchung der lokalen konvektiven Transportvorgänge auf Prallflächen. Ph.D. Thesis, Technische Hochschule Darmstadt.
Raffel, M., Willert, C., Werely, S., Kompenhans, J., 2007. Particle Image Velocimetry, second ed. Springer-Verlag, Berlin, Heidelberg.
Sturzebecher, D., Anders, S., Nitsche, W., 2001. The surface hot-wire as a means of measuring mean and fluctuating wall shear stress. Experiments in Fluids 31, 294–301.
Viskanta, R., 1993. Heat transfer to impinging isothermal gas and flame jets. Experimental Thermal and Fluid Science 6, 111–134.
Walker, J.D.A., Smith, C.R., Cerra, A.W., Doligalski, T.L., 1987. The impact of a vortex ring on a wall. Journal of Fluid Mechanics 181, 99–140.
Zaman, K., Hussain, A., 1980. Vortex pairing in a circular jet under controlled excitation. Part 1. General jet response. Journal of Fluid Mechanics 101, 449–491.
Zumbrunnen, D., Aziz, M., 1993. Convective heat transfer enhancement due to intermittency in an impinging jet. Journal of Heat Transfer 115, 91–98.